J|A|C|S
ARTICLES
Published on Web 01/24/2002

Dihydroazulene/Vinylheptafulvene Photochromism: A Model for One-Way Photochemistry via a Conical Intersection

Martial Boggio-Pasqua, Michael J. Bearpark, Patricia A. Hunt, and Michael A. Robb*

Contribution from the Department of Chemistry, King's College London, Strand, London WC2R 2LS, U.K.

Received May 9, 2001

Abstract: Dihydroazulene (DHA)/vinylheptafulvene (VHF) photochromism has been investigated by studying the isomerization of 1,2,3,8a,9-pentahydrocyclopent[a]azulene-9,9-dicarbonitrile through complete active space-self consistent field calculations on the ground (S_0) and first excited (S_1) states of smaller model compounds. In each case, the S_1 reaction coordinate is characterized by a transition structure for adiabatic ring opening, connecting a DHA-like intermediate to a much more stable VHF-like structure. This VHF-like structure is not a real S_1 minimum but a crossing (i.e., a conical intersection) between the excited- and ground-state potential energy surfaces. The existence of such a crossing is consistent with the lifetime of ~600 fs recently measured for the DHA-like intermediate on S_1 (Ern, J.; Petermann, M.; Mrozek, T.; Daub, J.; Kuldova, K.; Kryschi, C. *Chem. Phys.* **2000**, *259*, 331−337). The shape of the crossing is also crucial; it not only explains the fact that the quantum yield approaches 1.0 for the forward DHA → VHF reaction, but also the lack of any fluorescence or photochemical back-reaction from VHF. These findings are supported by ab initio direct dynamics calculations. This work suggests that calculating and understanding the topology of excited-state potential energy surfaces will be useful in designing photochromic molecules.

Introduction

Organic compounds with photochromic properties are of considerable interest at present, because of their potential applications for data storage and processing[1a,b] and molecular switching.[1c] Many have now been characterized,[2] including the dihydroazulene/vinylheptafulvene (DHA/VHF) couple,[3−5] for example, **1**, Scheme 1.[5]

This type of system has been intensively studied because it is an example of "one-way" photochromism; the photochemical rearrangement of DHA to VHF cannot be reversed by VHF absorption at a different frequency, but only by heat. Using femtosecond-resolved transient absorption spectroscopy, VHF formation has been detected[5] within 1.2 ps of the initial excitation of DHA **1**, and the speed of this reaction has been attributed to a conical intersection[6] between the ground and first excited states as shown in Figure 1.[5] In this paper, we confirm the existence of an intersection, but show that the shape of the surrounding potential energy surfaces is central to understanding the high quantum yield for the forward DHA → VHF reaction and the lack of any fluorescence or photochemical back-reaction from VHF. Despite the fact that any plot of energy against a single "reaction coordinate" will be misleading in some respect, we have also produced a revised Figure 1 (Figure 2) which is consistent with both the experiments[5] and the calculations we describe below.

Scheme 1

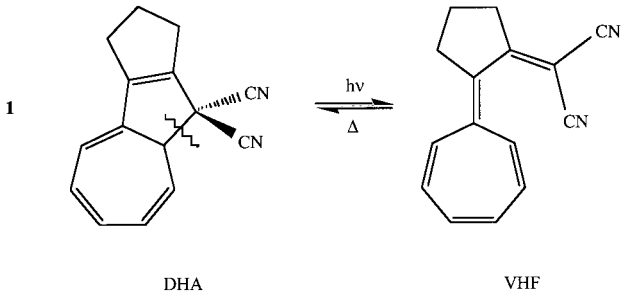

Several features of the excited-state potential energy surfaces of DHA and VHF can be inferred from experiment. Steady-state and time-resolved measurements on a series of DHA derivatives were carried out in 1993.[4] (We often use the generic labels "DHA" and "VHF" in what follows, as we are interested in features of the potential energy surfaces common to all such compounds.) These DHA derivatives were fluorescent: weakly

(1) (a) Irie, M. *Chem. Rev.* **2000**, *100*, 1685−1716. (b) Yokoyama, Y. *Chem. Rev.* **2000**, *100*, 1717−1739. (c) Mrozek, T.; Daub, J.; Ajayaghosh, A. *Optoelectronic Molecular Switches Based on Dihydroazulene-Vinylheptafulvene (DHA-VHF)*; Feringa, B. L., Ed.; Wiley-VCH: Weinheim, 2001; pp 63−106.
(2) Dürr, H., Bouas-Laurent, H., Eds. *Photochromism: Molecules and Systems*; Elsevier: Amsterdam, 1990.
(3) Daub, J.; Knochel, T.; Mannschreck, A. *Angew. Chem., Int. Ed. Engl.* **1984**, *23*, 960−961.
(4) Gorner, H.; Fischer, C.; Gierisch, S.; Daub, J. *J. Phys. Chem.* **1993**, *97*, 4110−4117.
(5) Ern, J.; Petermann, M.; Mrozek, T.; Daub, J.; Kuldova, K.; Kryschi, C. *Chem. Phys.* **2000**, *259*, 331−337.
(6) (a) Teller, E. *J. Phys. Chem.* **1937**, *41*, 109. (b) Teller, E. *Isr. J. Chem.* **1969**, *7*, 227−235. (c) Herzberg, G. *The Electronic Spectra of Polyatomic Molecules*; Van Nostrand: Princeton, 1966; p 442. (d) Salem, L. *Electrons in Chemical Reactions: First Principles*; Wiley: New York, 1982; pp 148−153. (e) Yarkony, D. R. *Acc. Chem. Res.* **1998**, *31*, 511−518. (f) Robb, M. A.; Garavelli, M.; Olivucci, M.; Bernardi, F. *Rev. Comput. Chem.* **2000**, *15*, 87−146.

10.1021/ja0161655 CCC: $22.00

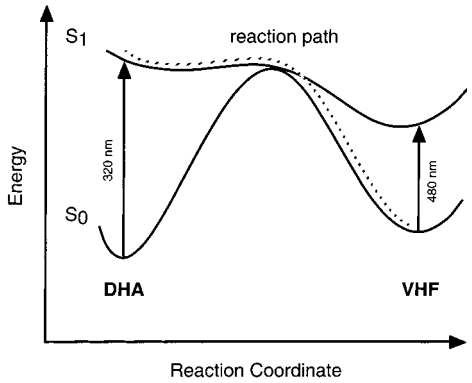

Figure 1. Outline of the S_1 and S_0 potential energy surfaces of DHA/VHF suggested by experiment, taken from ref 5.

in solution, but with quantum yields from 0.15 to 0.9 measured in low-temperature glass. In each case, the emission frequency was hardly affected by the solvent polarity, suggesting that there is a DHA-like minimum close to the Franck−Condon geometry on the potential energy surface of a valence $\pi\pi^*$ excited state of DHA. Decreased emission at higher temperatures is accompanied by increased DHA → VHF conversion, with measured quantum yields from 0.1 to 0.6.[4] These results are consistent with a shallow barrier on the excited state between the DHA-like minimum and VHF. A triplet mechanism for DHA → VHF conversion was ruled out because the VHFs were formed within the 50 ns time scale of the 1993 experiments. Furthermore, the sum of the quantum yields for the emission and photochemical reaction was typically less than 1.0,[4] suggesting that in some systems DHA(S_1) can decay back to DHA(S_0) nonradiatively before reaching VHF.

In contrast to DHA, no emission could be detected from VHF itself even at low temperature, suggesting that there is no corresponding excited-state minimum.[4] Figure 1 is misleading in this respect; as we shall show later (Figure 2), the lowest-energy point on S_1 actually has a VHF-like geometry, but one which corresponds to a conical intersection of ground and excited states rather than a minimum. Such a crossing explains the observed lack of fluorescence from VHF. Despite prolonged excitation, no photochemical back-reaction could be detected. Instead, VHF reverts to the more stable DHA thermally, with a measured activation barrier of ∼20 kcal mol^{-1} [4,5] giving a lifetime of a few hours at room temperature.

More recently, femtosecond-resolved transient absorption spectroscopy was used to study the DHA 1,2,3,8a,9-pentahydrocyclopent[a]azulene-9,9-dicarbonitrile (**1**, Scheme 1),[5] for which a quantum yield for conversion to VHF of nearly 1.0 was measured. The peak absorption of the DHA form of **1** is at 320 nm (89 kcal mol^{-1}), the VHF absorption peak is at 480 nm (60 kcal mol^{-1}), and the two bands barely overlap.[5] Two additional key observations were made. The first was direct detection of the postulated DHA-like intermediate on S_1, with an $S_1 \rightarrow S_n$ absorption centered at 700 nm (41 kcal mol^{-1}) reaching a maximum at 0.384 ps after the initial excitation of DHA. Second, the decay of this intermediate coincided with the appearance of VHF, with an absorption centered at 480 nm which had almost completely developed after 1.92 ps. The ring-opening reaction from DHA → VHF therefore takes place in approximately a picosecond, which is consistent with a conical intersection along the excited-state pathway from DHA to VHF.

In summary, there are two experimental observations which strongly suggest the presence of an S_1/S_0 conical intersection in DHA/VHF: the rapid, efficient photochemical conversion of DHA → VHF which has now been studied directly[5] and the lack of fluorescence at any temperature from VHF. The purpose of this work is to show that the *same* conical intersection is responsible for both observations, although it turns out that different regions of the crossing are involved in each case. Because of the shape of the potential energy surfaces in the region of this crossing, all reaction paths on the ground state lead to the VHF photoproduct (Figure 2), accounting for the high quantum yield of the photoisomerization process. Our model for DHA → VHF photochromism is based on dividing the excited-state potential energy surface into two distinct regions, with adiabatic breaking of a σ bond on the DHA side, leading to a nonadiabatic surface crossing on the VHF side. VHF itself behaves very much like fulvene, a prototype system we have previously studied.[7b,d]

These are the first calculations to be carried out on the excited states of DHA/VHF. We have chosen to study **1** as a prototype for the general DHA/VHF rearrangement, because of the detailed time-resolved data recently made available for this system.[5] However, because of the size of this molecule, we have used a series of smaller model compounds (**2a**−**2c**, Scheme 2) to make the excited-state calculations feasible.

The model system on which all of our work is based is **2a**. As compared to **1**, the two cyano groups have been removed, and the seven-membered ring has been reduced to five members. We have then separately investigated the effects of reintroducing the cyano groups (in **2b**) and expanding the five-membered ring back to seven (in **2c**). The fact that the topology of the ground- and excited-state potential energy surfaces is the same for all three model systems gives us confidence that we have a good description of the behavior of **1** itself.

This paper is organized as follows. Computational Methods describes the computational methods used and the choice of model systems (Scheme 2). The calculated potential energy surfaces and an interpretation of the experimental observations are presented in Results and Discussion. A justification of the model systems chosen to carry out this study is also given in this section, followed by the results of limited ab initio trajectory calculations. In the conclusion, we emphasize that the topology of the potential energy surfaces determined here for DHA/VHF will be found elsewhere and that calculating and understanding this topology will be useful in designing photochromic molecules with particular properties.

Computational Methods

First of all, we stress that an accurate evaluation of the reaction energetics is not within the scope of this work. We concentrate on the topology of the potential energy surfaces and the nature of the relevant reaction paths on these surfaces.

The process studied in this work (Scheme 1) involves a σ bond breaking, followed by the complete reorganization of the electronic

(7) (a) Bearpark, M. J.; Bernardi, F.; Clifford, S.; Olivucci, M.; Robb, M. A.; Smith, B. R.; Vreven, T. *J. Am. Chem. Soc.* **1996**, *118*, 169−175. (b) Bearpark, M. J.; Bernardi, F.; Olivucci, M.; Robb, M. A.; Smith, B. R. *J. Am. Chem. Soc.* **1996**, *118*, 5254−5260. (c) Bearpark, M. J.; Robb, M. A.; Yamamoto, N. *Spectrochim. Acta, Part A* **1999**, *55*, 639−646. (d) The topology of the ground- and excited-state surfaces of VHF and fulvene is similar, but the substituent effects are different; VHF is stabilized by electron-withdrawing groups at C-10 and fulvene is stabilized by electron-donating groups at C-6, and this will affect the energetics differently (Daub, J.; *Chimia* **1987**, *41*, 52−59).

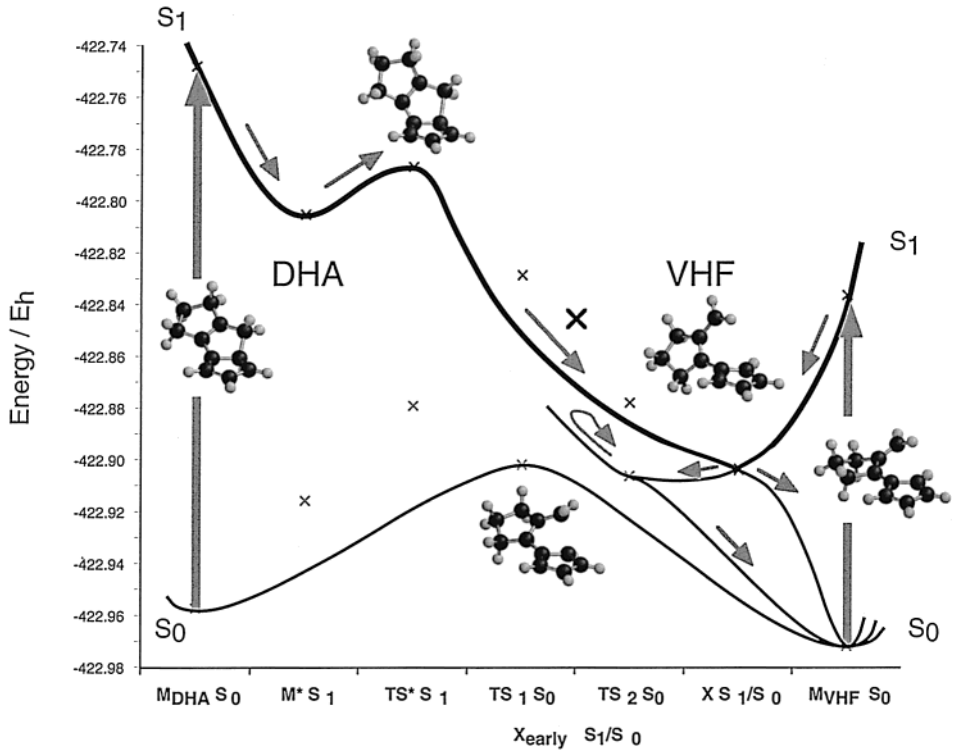

Figure 2. A revised outline of reaction paths on the S_1 and S_0 potential energy surfaces of DHA/VHF, based on the calculations presented here (for the model system **2a** described in the Computational Details section). The asymmetry between DHA and VHF is clear; all reaction paths on the excited state lead to VHF on S_0 via a conical intersection. (**M** = minimum; **TS** = transition structure; **X** = S_1/S_0 conical intersection. Reaction paths on S_1 are indicated in bold.)

Scheme 2

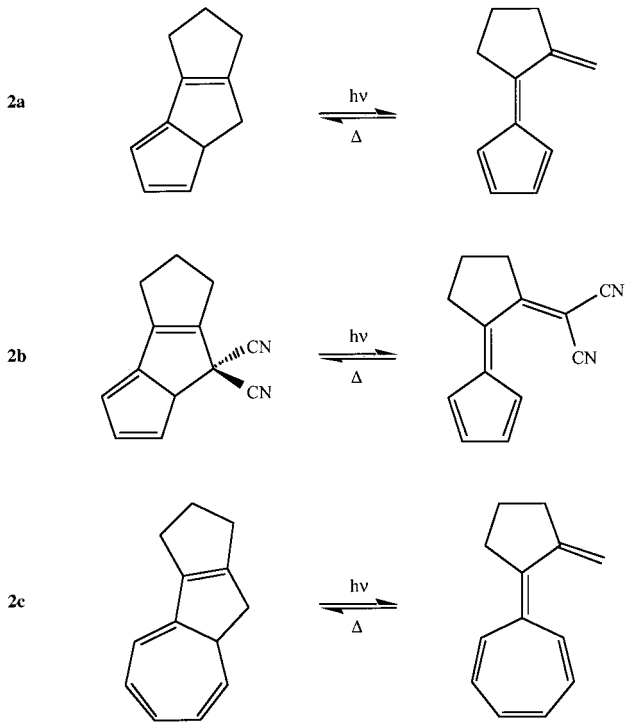

π-system of a valence excited state. For a reliable description of these potential energy surfaces, a computational method that accounts for all of the important electronic rearrangements is required. We have used the complete active space-self consistent field (CASSCF) method, which is currently the most appropriate ab initio method for calculating the excited states of such a system. The most critical feature of this kind of calculation is the choice of the active space (orbitals which can have variable occupancies between 2.0 and 0.0). To describe the S_1 state of DHA/VHF, the obvious choice of active space would be 10 electrons in 10 molecular orbitals. (For DHA, two active orbitals describe the σ bond which is broken.) Computations with such large active spaces are currently too expensive for the full exploration of potential energy surfaces, and we have therefore carried out calculations on several smaller but closely related model systems, as shown in Scheme 2: (**2a**) five-membered ring hydrocarbon only, (**2b**) five-membered ring + cyano groups, and (**2c**) seven-membered ring hydrocarbon only.

Previous calculations suggested that the five- and seven-membered rings would be electronically interchangeable,[7a–c] both having an odd number of electrons without being significantly strained. We checked this by comparing our results for model compounds **2a** and **2c**. Being able to reduce the size of the active space to the eight electrons in eight orbitals necessary for **2a** speeds up the CASSCF calculations by several orders of magnitude and also makes analytical frequency calculations possible. Next, by comparing model compounds **2a** and **2b**, we found that including the cyano groups did not affect the reaction paths we have studied qualitatively (see Results and Discussion, subsection V). These groups are necessary for the observed photochromic behavior to prevent side reactions such as hydrogen migration, which we have not studied, from being favored.[8] Since neither changing the ring size nor adding cyano groups affects the topology of the potential energy surface individually, we do not expect both combined to do so. We therefore believe that our calculations on model system **2a** (Scheme 2) give us a faithful representation of the potential energy surfaces of the title compound **1** (Scheme 1). We have used model **2a** for the majority of the calculations that follow, labeling the different regions of the potential energy surface as DHA or VHF as if we were studying compound **1** directly.

We have only considered singlet states in our calculations, because the triplet states were not found to be involved in the DHA → VHF

(8) Daub, J., private communication.

photoconversion experimentally.[4] In addition, we have only calculated the first singlet excited-state S_1 with CASSCF, as the gap between this and the next excited singlet was found to be large experimentally (~40 kcal mol^{-1} at the S_1 minimum[5]). All of the critical points on the potential energy surfaces of the ground and excited states of the model system **2a** were initially optimized with the 4-31G basis set. Minima and transition structures were characterized with analytical frequency calculations using the same basis.

The conical intersection was optimized using the algorithm described in ref 9. (State-averaged orbitals were used. In the case of **2c**, the orbital rotation derivative correction to the gradient was not computed.) This gives the lowest-energy point on the crossing, at which there are two coordinates, the gradient difference and derivative coupling vectors (branching space),[6,10] which lift the degeneracy. The remaining 3N-8 coordinates (intersection space) preserve the degeneracy, which therefore persists over a wide range of molecular geometries (see, e.g., ref 7b). Decay can take place away from the minimum energy point on the crossing if a higher-energy crossing region is encountered first, and our calculations suggest that this is true for the forward DHA → VHF reaction.

All critical points located using the 4-31G basis for model system **2a** were reoptimized with cc-pVDZ[11] to assess the sensitivity of these structures and their relative energies to the inclusion of polarization functions in the basis set. No significant changes were found; no bond lengths changed by more than ±0.01 Å. Density functional calculations (B3LYP[12a]/cc-pVDZ) were also carried out on the two S_0 minima of **1** and **2a**−**2c** as a check on the relative energetics. These were followed by time-dependent density functional theory calculations (TDDFT[12b,c] using B3LYP/cc-pVDZ) to ensure that the nature of the $S_0 \rightarrow S_1$ transition involved is the same in the three model systems **2a**−**2c** and the real system **1** (see Results and Discussion, subsection V).

The 4-31G basis was then used to determine the pathways linking all of the critical points located with CASSCF. Initially, linear interpolations were carried out on the ground and excited states. Intrinsic reaction coordinates were then calculated from all transition structures. Reaction paths on S_0 leading down from the conical intersection were calculated using the constrained optimization algorithm described in ref 13. This initial reaction direction (IRD) search for steepest descent directions from a singularity enables reaction paths to be located without having to compute force constants, starting at points on a potential energy surface where the gradient is not zero. The same IRD method was also used to locate reaction paths from the vertically excited DHA and VHF geometries on the excited state.

Finally, ab initio direct dynamics calculations[14,15] coupled with surface hopping have been performed for **2a**. In such a procedure, the first and second derivatives are computed at each point along the trajectory which is presently very time-consuming (each of the two model trajectories described here took ~600 h to calculate). The nonadiabatic surface hop in the crossing region is determined by propagating the solutions of the time-dependent electronic Schrödinger equation in concert with nuclear propagation. The relative population of the two states of interest is used to determine when a hop occurs.

All of the CASSCF calculations described here were performed with development versions of Gaussian 99.[16]

Scheme 3

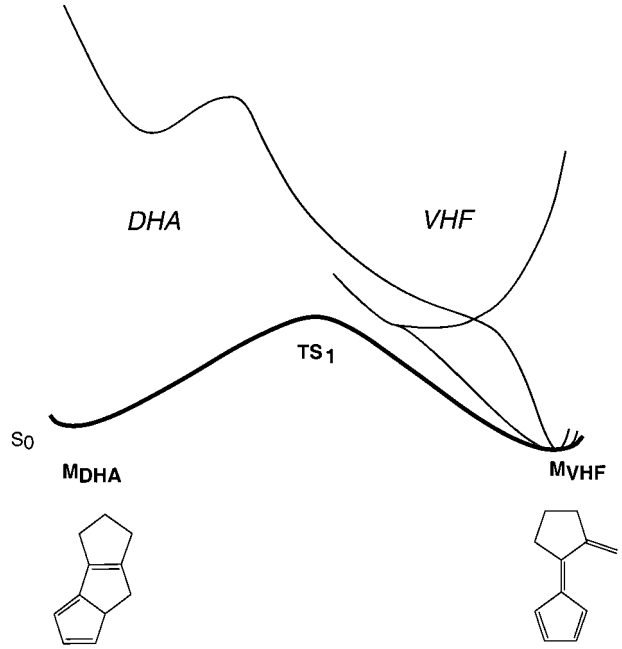

Results and Discussion

This section is divided into six subsections I−VI. In the first three, we discuss the structures and reaction pathways located on the ground (S_0)- and excited (S_1)-state potential energy surfaces of the model system **2a** (Scheme 2) which have been summarized in Figure 2. These structures are shown in detail in Figures 3−7, and the energetics are given in Tables 1 (4-31G basis) and 2 (cc-pVDZ basis). We discuss the ground state first, followed by the reaction pathways on S_1 from DHA and VHF in turn. (Figures S1−S7 that summarize the reaction path calculations themselves are available as Supporting Information.) The fourth subsection discusses the origin of the conical intersection. In the fifth subsection, we justify the choice of model system **2a** by showing that the potential energy surfaces of **2a**, **2b**, and **2c** (Scheme 2) have the same topology and vertical excitation leads to the same S_1 state for these systems and **1**. Dynamics calculations on **2a** are then discussed in subsection VI.

I. S_0 Potential Energy Surface. Two minima corresponding to DHA ($\mathbf{M_{DHA}}$) and VHF ($\mathbf{M_{VHF}}$) and a transition structure connecting them ($\mathbf{TS_1}$) were located on the ground-state potential energy surface of **2a**, as shown in Figure 2/Scheme 3 and Figure 3. The reaction coordinate leading to the VHF product involves

(9) (a) Ragazos, I. N.; Robb, M. A.; Bernardi, F.; Olivucci, M. *Chem. Phys. Lett.* **1992**, 197, 217−223. (b) Bearpark, M. J.; Robb, M. A.; Schlegel, H. B. *Chem. Phys. Lett.* **1994**, 223, 269−274.
(10) Atchity, G. J.; Xantheas, S. S.; Ruedenberg, K. *J. Chem. Phys.* **1991**, *95*, 1862−1876.
(11) Dunning, T. H. *J. Chem. Phys.* **1989**, *90*, 1007−1023.
(12) (a) Becke, A. D. *J. Chem. Phys.* **1993**, *98*, 5648−5652. (b) Bauernschmitt, R.; Ahlrichs, R. *Chem. Phys. Lett.* **1996**, *256*, 454−464. (c) Stratmann, R. E.; Scuseria, G. E.; Frisch, M. J. *J. Chem. Phys.* **1998**, *109*, 8218−8224.
(13) (a) Celani, P.; Robb, M. A.; Garavelli, M.; Bernardi, F.; Olivucci, M. *Chem. Phys. Lett.* **1995**, *243*, 1−8. (b) Garavelli, M.; Celani, P.; Fato, M.; Bearpark, M. J.; Smith, B. R.; Olivucci, M.; Robb, M. A. *J. Phys. Chem. A* **1997**, *101*, 2023−2032.
(14) (a) Helgaker, T.; Uggerud, E.; Jensen, H. J. Aa. *Chem. Phys. Lett.* **1990**, *173*, 145−150. (b) Chen, W.; Hase, W. L.; Schlegel, H. B. *Chem. Phys. Lett.* **1994**, *228*, 436−442. (c) Warshel, A.; Karplus, M. *Chem. Phys. Lett.* **1975**, *32*, 11. (d) Smith, B. R.; Bearpark, M. J.; Robb, M. A.; Bernardi, F.; Olivucci, M. *Chem. Phys. Lett.* **1995**, *242*, 27−32. (e) Klein, S.; Bearpark, M. J.; Smith, B. R.; Robb, M. A.; Olivucci, M.; Bernardi, F. *Chem. Phys. Lett.* **1998**, *292*, 259−266.
(15) Vreven, T. Ph.D. Thesis, King's College, University of London, 1998.
(16) Frisch, M. J.; Trucks, G. W.; Schlegel, H. B.; Scuseria, G. E.; Robb, M. A.; Cheeseman, J. R.; Zakrzewski, V. G.; Montgomery, J. A., Jr.; Stratmann, R. E.; Burant, J. C.; Dapprich, S.; Millam, J. M.; Daniels, A. D.; Kudin, K. N.; Strain, M. C.; Farkas, O.; Tomasi, J.; Barone, V.; Cossi, M.; Cammi, R.; Mennucci, B.; Pomelli, C.; Adamo, C.; Clifford, S.; Ochterski, J.; Petersson, G. A.; Ayala, P. Y.; Cui, Q.; Morokuma, K.; Malick, D. K.; Rabuck, A. D.; Raghavachari, K.; Foresman, J. B.; Ortiz, J. V.; Baboul, A. G.; Cioslowski, J.; Stefanov, B. B.; Liu, G.; Liashenko, A.; Piskorz, P.; Komaromi, I.; Gomperts, R.; Martin, R. L.; Fox, D. J.; Keith, T.; Al-Laham, M. A.; Peng, C. Y.; Nanayakkara, A.; Gonzalez, C.; Challacombe, M.; Gill, P. M. W.; Johnson, B.; Chen, W.; Wong, M. W.; Andres, J. L.; Gonzalez, C.; Head-Gordon, M.; Replogle, E. S.; Pople, J. A. *Gaussian 99*, Development Version, revision B.01; Gaussian, Inc., Pittsburgh, PA, 1998.

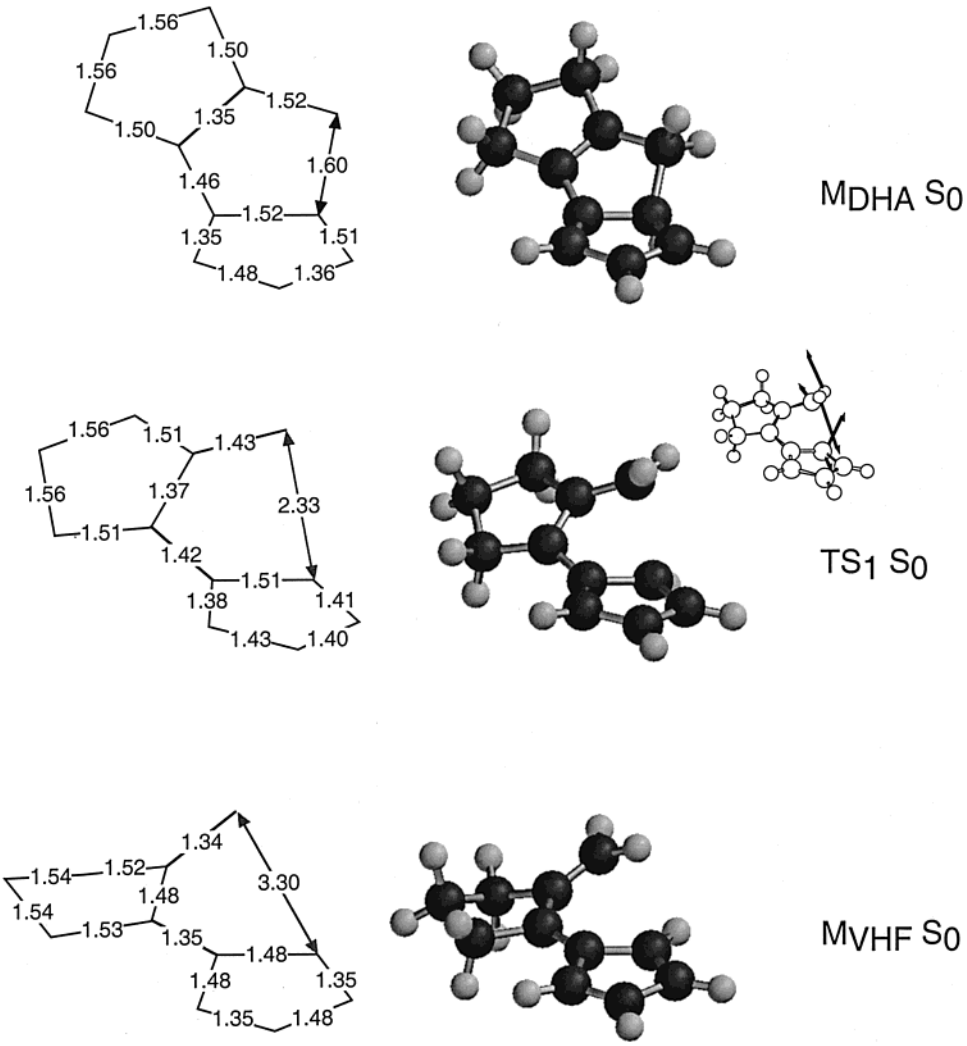

Figure 3. Two minima ($\mathbf{M_{DHA}}$, $\mathbf{M_{VHF}}$) corresponding to DHA and VHF on the S_0 potential energy surface and the transition structure ($\mathbf{TS_1}$) connecting them, located with CASSCF/cc-pVDZ. All bond lengths are in Å; 4-31G bond lengths agree to within ±0.01 Å. Energies are in Tables 1 and 2. The transition vector associated with $\mathbf{TS_1}$ is shown in the inset.

Table 1. CASSCF(8,8)/4-31G Energies on the 5-Carbon Ring System **2a** (Scheme 2) at 4-31G Optimized Geometries (Figures 3−7)[a]

geometry	figure	S_0/E_h	S_1/E_h	$\Delta E(S_1-S_0)$ /kcal mol^{-1}	$\Delta E(S_0)$ /kcal mol^{-1}	$\Delta E(S_1)$ /kcal mol^{-1}
$\mathbf{M_{DHA}\ S_0}$	3	−422.96151	−422.75000	132.7	0.0	35.4
		−422.95695	*−422.74788*	*131.2*	*0.0*	*35.8*
$\mathbf{TS_1\ S_0}$	3	−422.90448	−422.83044	46.5	35.8	−15.0
		−422.90189	*−422.82850*	*46.1*	*34.6*	*−14.8*
$\mathbf{M_{VHF}\ S_0}$	3	−422.97551	−422.83855	85.9	−8.8	−20.1
		−422.97154	*−422.83596*	*85.1*	*−9.2*	*−19.4*
M* S_1	4	−422.91783	−422.80646	69.9	27.4	0.0
		−422.91550	*−422.80499*	*69.3*	*26.0*	*0.0*
TS* S_1	4	−422.88203	−422.78896	58.4	49.9	11.0
		−422.87880	*−422.78655*	*57.9*	*49.0*	*11.6*
X S_1/S_0	5	*−422.90383*	*−422.90351*	*0.2*	*33.3*	*−61.8*
$\mathbf{X_{early}\ S_1/S_0}$	6	*−422.84489*	*−422.84481*	*<0.1*	*70.3*	*−25.0*
$\mathbf{TS_2\ S_0}$	7	−422.90783	−422.87919	18.0	33.7	−45.6
		−422.90600	*−422.87756*	*17.8*	*32.0*	*−45.5*
$\mathbf{TS_3\ S_0}$	7	−422.91011	−422.87679	20.9	32.3	−44.1
		−422.90833	*−422.87508*	*20.9*	*30.5*	*−44.0*

[a] **M** = minimum; **TS** = transition structure; **X** = conical intersection. State-averaged energies in italics. $\Delta E(S_0)$ and $\Delta E(S_1)$ are calculated with the $\mathbf{M_{DHA}\ S_0}$ and **M* S_1** energies, respectively, as references.

simultaneous σ-bond breaking and the complete reorganization of the π-electronic system.

For **2a**, $\mathbf{M_{VHF}}$ was calculated to be the lowest-energy structure on S_0 by ∼4 kcal mol^{-1} (CASSCF/cc-pVDZ, Table 2). This disagrees with the experiment[4] which shows that the DHA isomer is thermochemically more stable than VHF for all such compounds studied so far. However, these were all seven-membered ring compounds such as **1**, and as far as we are

Table 2. CASSCF(8,8)/cc-pVDZ Energies on the 5-Carbon Ring System **2a** (Scheme 2) at cc-pVDZ Optimized Geometries (Figures 3−7)[a]

geometry	figure	S_0/E_h	S_1/E_h	$\Delta E(S_1-S_0)$ /kcal mol^{-1}	$\Delta E(S_0)$ /kcal mol^{-1}	$\Delta E(S_1)$ /kcal mol^{-1}
$\mathbf{M_{DHA}}$ $\mathbf{S_0}$	3	−423.60461	−423.39272	133.0	0.0	36.2
		−423.59854	*−423.38981*	*131.0*	*0.0*	*36.8*
$\mathbf{TS_1}$ $\mathbf{S_0}$	3	−423.54188	−423.46824	46.2	39.4	−11.2
		−423.53862	*−423.46580*	*45.7*	*37.6*	*−10.8*
$\mathbf{M_{VHF}}$ $\mathbf{S_0}$	3	−423.61103	−423.47689	84.2	−4.0	−16.6
		−423.60594	*−423.47343*	*83.2*	*−4.6*	*−15.6*
M* $\mathbf{S_1}$	4	−423.56123	−423.45042	69.5	27.2	0.0
		−423.55802	*−423.44851*	*68.7*	*25.4*	*0.0*
TS* $\mathbf{S_1}$	4	−423.52201	−423.43186	56.6	51.8	11.6
		−423.51711	*−423.42800*	*55.9*	*51.1*	*12.9*
X $\mathbf{S_1/S_0}$	5	*−423.53800*	*−423.53787*	*<0.1*	*38.0*	*−56.1*
$\mathbf{TS_2}$ $\mathbf{S_0}$	7	−423.54408	−423.51611	17.6	38.0	−41.2
		−423.54172	*−423.51396*	*17.4*	*35.7*	*−41.1*
$\mathbf{TS_3}$ $\mathbf{S_0}$	7	−423.54613	−423.51389	20.2	36.7	−39.8
		−423.54381	*−423.51166*	*20.2*	*34.3*	*−39.6*

[a] **M** = minimum; **TS** = transition structure; **X** = conical intersection. State-averaged energies in italics. $\Delta E(S_0)$ and $\Delta E(S_1)$ are calculated with the $\mathbf{M_{DHA}}$ $\mathbf{S_0}$ and **M*** $\mathbf{S_1}$ energies, respectively, as references.

Table 3. B3LYP/cc-pVDZ Energies at Optimized Geometries (Supporting Figure S13) of the Two S_0 Minima ($\mathbf{M_{DHA}}$, $\mathbf{M_{VHF}}$) of Systems (Schemes 1 and 2) Studied in This Paper

system	$\mathbf{M_{DHA}}$ S_0/E_h	$\mathbf{M_{VHF}}$ S_0/E_h	ΔE(VHF−DHA) /kcal mol^{-1}
1	−688.26182	−688.26634	−2.84
2a	−426.35673	−426.35360	1.96
2b	−610.83338	−610.84187	−5.33
2c	−503.78697	−503.76466	14.00

aware, there is no experimental data for the five-membered ring compound **2a** itself. Furthermore, our calculations are not accurate enough for converged energetics, and the energy differences involved are small. Using the density functional method B3LYP/cc-pVDZ (Table 3) and reoptimizing geometries, we find that the DHA isomer with **2a** is ∼2 kcal mol^{-1} more stable than VHF. Given this disagreement, we cannot say for certain which isomer, DHA or VHF, is lower in energy for **2a**, but since the main conclusions of this paper concerning the excited-state reaction paths are unaffected, we decided not to pursue this point further. (The corresponding energy differences for **2b** and **2c** are discussed in subsection V.)

Figure 3 shows that $\mathbf{M_{DHA}}$ has three double bonds (∼1.35 Å) as expected and that $\mathbf{M_{VHF}}$ has four. For $\mathbf{M_{DHA}}$, the σ bond that breaks to give VHF is the longest at 1.60 Å, longer than expected. It was thought that this could be an artifact of the CASSCF method. This is because the p orbitals included in the active space to describe this bond are necessary for VHF, where they become part of the π-system, but not for DHA, as the occupancies are very close to two and zero there. However, this bond was also calculated to be among the longest with density functional theory; the B3LYP/cc-pVDZ value is 1.56 Å (Figure S13). The conclusion is that it is a long bond, exaggerated by ∼0.03 Å with CASSCF.

II. S_1 DHA → VHF Pathway. Since there are no experimental results available for compound **2a** itself, we cannot calibrate our excitation energies directly. However, the S_1 state of DHA/VHF is a valence $\pi\pi^*$ excited state, with no ionic/Rydberg character, and on the basis of previous calculations[17] we expect it to be well described with CASSCF. (This is supported by the TDDFT calculations presented in subsection V.)

(17) Serrano-Andrés, L.; Merchan, M.; Nebot-Gil, I.; Lindh, R.; Roos, B. O. *J. Chem. Phys.* **1993**, *98*, 3151−3162.

Scheme 4

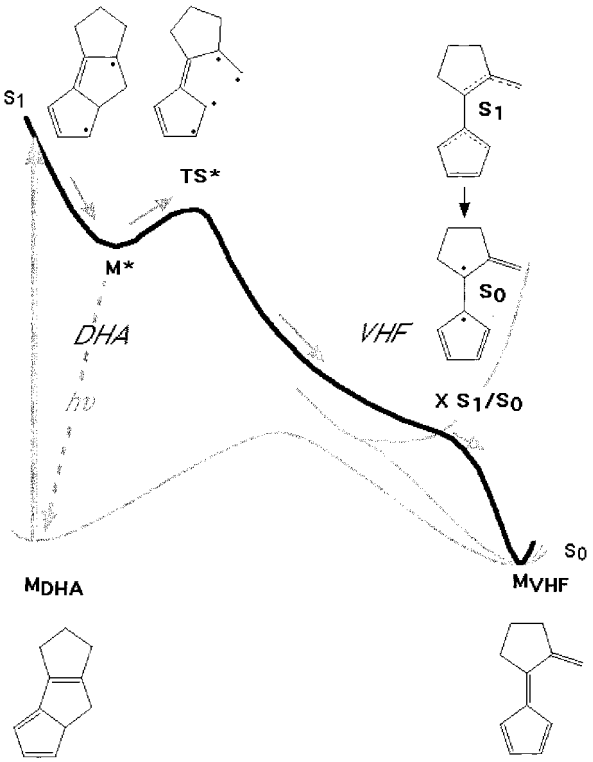

Table 2 shows that, at the $\mathbf{M_{DHA}}$ geometry on S_0, the S_0-S_1 gap is ∼133 kcal mol^{-1} (vertical excitation). Initial relaxation from this point on S_1 proceeds in two steps. First, there is a complete inversion of single and double bonds within the π-system, leading to a diradicaloid minimum **M*** (Figure 4 and Scheme 4/Figure 2), which is 36 kcal mol^{-1} lower in energy. The long σ bond which breaks to give VHF is unchanged at **M***, but increases to 1.88 Å as part of a second step, which leads to the transition structure **TS***. This transition structure is 11 kcal mol^{-1} above the minimum, but 24 kcal mol^{-1} below the vertical excitation energy (Table 2). Vertical excitation and/or higher temperatures will therefore produce sufficient kinetic energy to overcome the **TS*** barrier; 0−0 excitation and lower temperatures will favor fluorescence from **M*** as observed experimentally[4] (Scheme 4). Figure 4 shows that the two

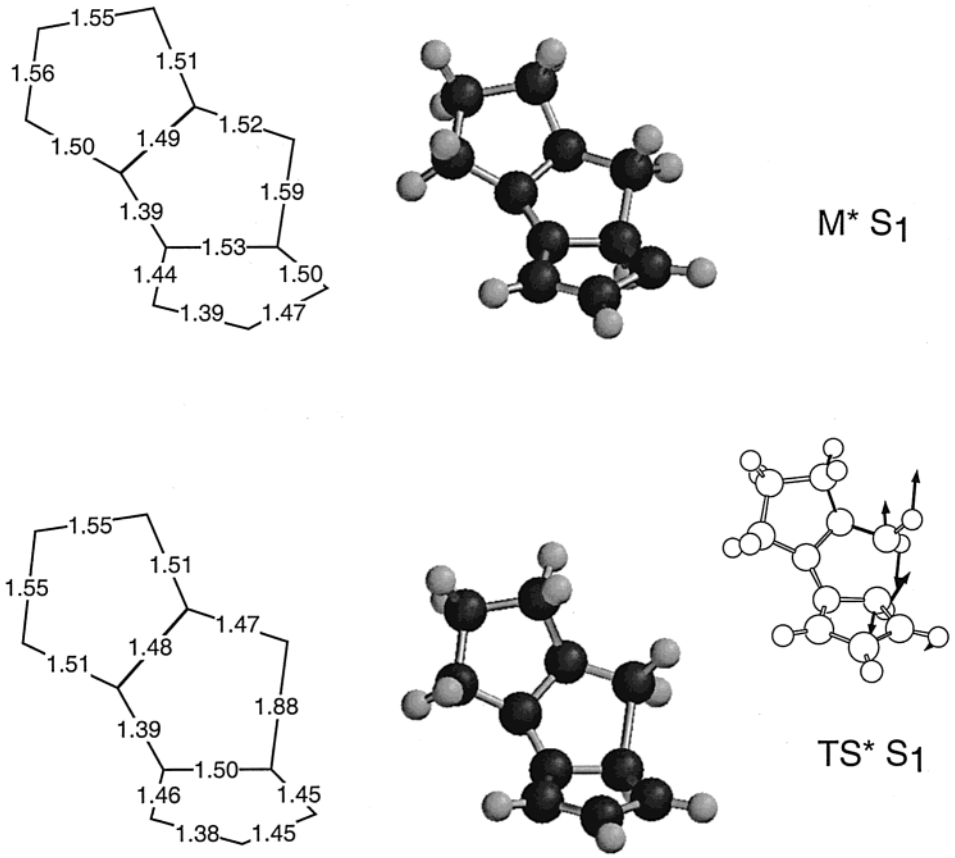

Figure 4. The DHA-like minimum (**M***) located on the S_1 potential energy surface with CASSCF/cc-pVDZ, and the transition structure (**TS***) leading toward VHF. All bond lengths are in Å; 4-31G bond lengths agree to within ±0.01 Å. Energies are in Tables 1 and 2. The transition vector associated with **TS*** is shown in the inset.

relaxation steps just described are almost completely decoupled: the π-system changes first, then the σ-bond.

The transition vector at **TS*** is dominated by adiabatic σ bond breaking. However, **TS*** is not a transition structure for adiabatic DHA ↔ VHF isomerization as no minimum corresponding to VHF could be found on S_1. The lowest-energy point on S_1 is VHF-like; it is not a minimum but rather a conical intersection between S_1 and S_0 (**X**, Figure 5) over 50 kcal mol^{-1} below **M***. (Tables 1 and 2 show that **X** actually has about the same energy on S_0 as the transition structure $\mathbf{TS_1}$ for VHF → DHA conversion.) Nonradiative decay to S_0 will be efficient at such a crossing, which is consistent with the observed lack of fluorescence from DHA at higher temperatures once **TS*** is overcome.[4,5]

The IRC calculated from **TS*** in the VHF direction does not actually reach **X** itself, the lowest-energy point optimized on the intersection. Instead, the IRC terminates at $\mathbf{X}_{early}$ (Figure 6), a point where S_1 and S_0 are degenerate which is over 30 kcal mol^{-1} above **X** (Table 1). There are two reasons for this. First, the crossing extends over a wide range of geometries. This can be understood by looking at the gradient difference and derivative coupling vectors at **X** itself (Figure 5). These are the directions that lift the S_1/S_0 degeneracy, and they are dominated by rearrangements of the fulvene ring alone. They do not involve either the σ bond which has broken or twisting about the remaining σ bond linking the two rings. The crossing will therefore persist for a wide range of values of these two coordinates, including $\mathbf{X}_{early}$. Second, the reaction coordinate leading to $\mathbf{X}_{early}$ from **TS*** is dominated by the σ bond which has broken, as shown by the transition vector computed at **TS*** (Figure 4). Because the minimum energy path from **TS*** on S_1 (Figure 4) is orthogonal to the directions that lift the S_1/S_0 degeneracy (Figure 5), it does not have to lead to the lowest energy point on the crossing but can terminate at a higher energy point. For molecules which are approximately thermally equilibriated (e.g., in solution), $S_1 \rightarrow S_0$ decay is normally expected to occur in the region of the crossing minimum. For DHA/VHF, it appears that this is not the case. Decay from the DHA side will *always* take place in a higher energy region of the crossing, because the S_1 reaction path is not in the plane which lifts the degeneracy at **X**.

To establish the products which can be formed after decay at $\mathbf{X}_{early}$, the initial relaxation directions (IRDs) were calculated (as described in the Computational Methods). Two distinct pathways were found, leading to the two S_0 minima $\mathbf{M_{DHA}}$ and $\mathbf{M_{VHF}}$. This means that, in principle, decay at $\mathbf{X}_{early}$ after the initial excitation of DHA can lead to regeneration of DHA as well as formation of the product VHF. This does not contradict the experimental result that once VHF has been reached, DHA cannot be regenerated photochemically. However, for "outstanding" DHAs such as the title compound **1**[5] (for which the quantum yield for DHA → VHF conversion approaches 1.0), nonradiative decay to give DHA(S_0) is highly unlikely. We believe that this is because the reaction is highly exothermic and that once the σ bond breaks past **TS***, the rapidly increasing kinetic energy will keep this bond length increasing at the crossing and lead on to VHF on S_0 rather than back to DHA. This is supported by the dynamics calculations in subsection

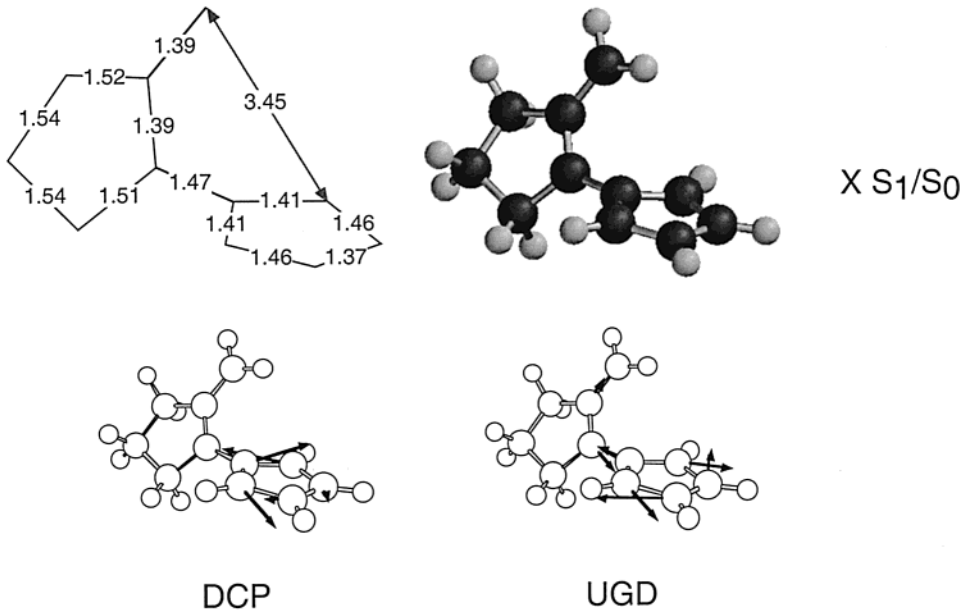

Figure 5. The lowest-energy point on the VHF-like conical intersection (**X**) between S_1 and S_0 located with CASSCF/cc-pVDZ. All bond lengths are in Å; 4-31G bond lengths agree to within ±0.01 Å. Energies are in Tables 1 and 2. The derivative coupling (DCP) and gradient difference (UGD) vectors, which lift the degeneracy at the crossing, are also shown in the inset.

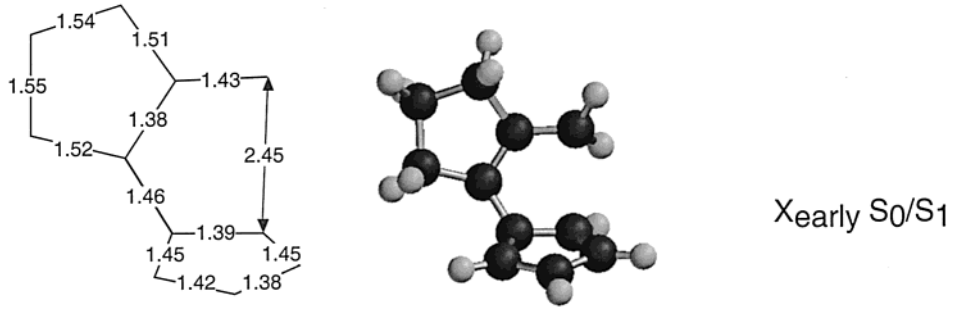

Figure 6. A higher-energy point ($\mathbf{X}_{early}$) on the S_1/S_0 conical intersection (CASSCF/4-31G), at which the IRC from **TS*** terminates. All bond lengths are in Å. Energies are in Table 1.

VI and shows that the existence of a reaction pathway is no guarantee that it will be followed.

III. S_1 VHF → VHF (Photophysical) Pathway. We now turn to VHF itself, to explain why there is no photochemical reaction back to DHA.

At the $\mathbf{M_{VHF}}$ geometry on S_0, Table 2 shows that the S_0-S_1 gap is ∼94 kcal mol^{-1} (vertical excitation). This value is ∼50 kcal mol^{-1} smaller than that for $\mathbf{M_{DHA}}$, which reflects the difference in the number of conjugated π electrons for both systems (6 π for $\mathbf{M_{DHA}}$; 8 π for $\mathbf{M_{VHF}}$ for **2a**).

The gradient on S_1 at the $\mathbf{M_{VHF}}$ geometry (Figure 2/Scheme 5) is very steep and directed toward the S_1/S_0 crossing **X** (Figure 5). This reaction path was calculated using the IRD method, and unlike DHA, no higher-energy crossing point was reached. Comparing Figures 3 and 5 shows that from $\mathbf{M_{VHF}} \rightarrow \mathbf{X}$, double and single bonds have inverted within the fulvene ring, which retains C_{2v} symmetry. In other words, the reaction coordinate defining the $\mathbf{M_{VHF}} \rightarrow \mathbf{X}$ path on S_1 is the same as the gradient difference vector at **X**. Unlike the reaction coordinate characterizing the $\mathbf{TS^*} \rightarrow \mathbf{X}_{early}$ path (subsection II) from DHA, the $\mathbf{M_{VHF}} \rightarrow \mathbf{X}$ reaction path involves one of the coordinates defining the branching space. Consequently, the minimum energy path on S_1 is naturally driven to the minimum energy crossing point **X**.

Scheme 5

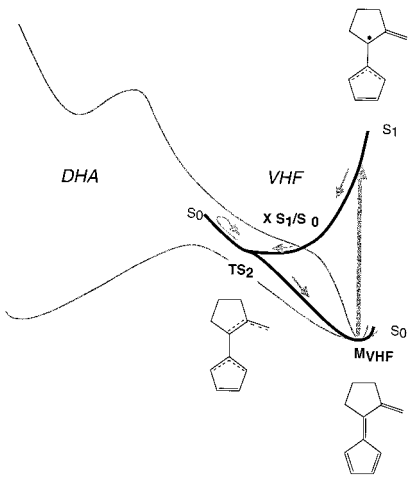

(Other relaxation paths on S_1 are ruled out for VHF as only one ground-state conformer could be located.) As we shall see later, this asymmetric topology of the S_1 potential energy surface accounts for the extraordinary properties of the DHA/VHF photochromic system.

The crossing **X** is the lowest-energy point on S_1 (Table 2), which explains the complete lack of fluorescence from VHF.

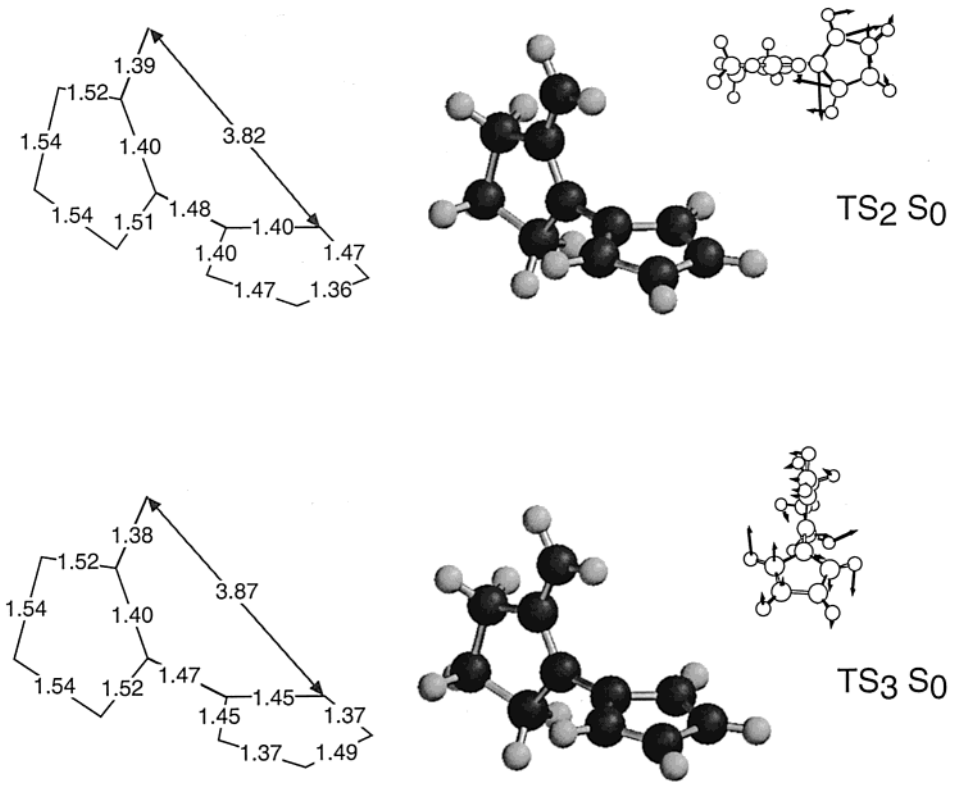

Figure 7. Transition structures (**TS$_2$**, **TS$_3$**) on S_0 in the vicinity of the S_1/S_0 conical intersection (CASSCF/cc-pVDZ). All bond lengths are in Å; 4-31G bond lengths agree to within ±0.01 Å. Energies are in Tables 1 and 2. The transition vectors are shown in the inset. (**TS$_3$** not shown in Figure 2, as it is so close in energy to **TS$_2$**.)

Contrast this with the behavior of a related system, azulene,[7a] in which there is a shallow minimum adjacent to the S_1/S_0 crossing, which leads to extremely weak but detectable[18] fluorescence.

Initial reaction directions were computed in the vicinity of **X** on S_0, to locate reaction paths towards ground-state products. Only one well-defined direction was located, which led back toward **M$_{VHF}$**. This was a surprise, as kinetic energy developed by relaxation from the **M$_{VHF}$** geometry on S_1 would be expected to lead in the opposite direction, and possibly to DHA. A more careful IRD search[19] eventually located a second pathway from **X** on S_0, terminating at the point **TS$_2$** (Figure 7) only ∼2 kcal mol^{-1} below **X**. **TS$_2$** has a very similar geometry to **X** and is the lowest point on the reaction path leading from **M$_{VHF}$** through **X** onto S_0. Continuing on the same path through **TS$_2$** leads to a steep rise in energy (Scheme 5/Figure 2), and molecules approaching **X** from the VHF side will therefore be reflected from this barrier back toward **M$_{VHF}$**.

TS$_2$ is a transition structure, but not along the reaction path we have just considered. Figure 7 shows that the transition vector at **TS$_2$** is essentially the same as the derivative coupling vector at **X**: dominated by the asymmetric recoupling of π-electrons within the fulvene ring and not involving any torsion about the σ bond linking the two rings. This is orthogonal to the reaction path from **M$_{VHF}$** on S_1 considered in the previous paragraph, which is parallel to the gradient difference vector at **X**.

An IRC calculation run from **TS$_2$** crashed after little change in energy. A force constant calculation at the crash geometry showed that the original **TS$_2$** transition vector had been lost, with torsion between the two rings now the downward direction. A search for a transition structure from this point revealed **TS$_3$** (Figure 7), which is only ∼1 kcal mol^{-1} below **TS$_2$**. At **TS$_3$**, the fulvene ring geometry is very similar to that of **M$_{VHF}$** (a large change in geometry from **TS$_2$** for little change in energy), and the transition vector is dominated by torsion between the two rings. The IRC from **TS$_3$** terminated at the two equivalent **M$_{VHF}$** minima (mirror images) in both directions. The S_0 potential energy surface appears to be very flat in the **TS$_2$**/**TS$_3$** region and is difficult to map precisely. We cannot be certain that there are not any other points similar to **TS$_2$**/**TS$_3$** (which have been found in other related systems[7b,7c]).

The most significant finding here is that both relaxation paths from **X** on S_0 lead to the VHF minimum **M$_{VHF}$**: one directly, and the other indirectly via in-plane ring rearrangement at **TS$_2$** (which breaks the symmetry of the fulvene ring) and torsion at **TS$_3$** (which preserves it). This explains the problem with the initial search for relaxation directions from **X**; at a certain distance from the crossing, there is effectively only one relaxation path. Moreover, no pathway to DHA was found. To visualize the shape of the potential energy surfaces in the region of the crossing, we generated a grid of geometries through linear interpolations along the (orthogonal) gradient difference and derivative coupling vectors, starting at **X**. S_0 and S_1 energies were calculated at each point on this grid, and the results are plotted in Figure 8.

The top view of Figure 8 shows that the S_0 surface around the crossing slopes downward to VHF in all directions. The closeup (bottom of Figure 8) shows the only small exception: the **TS$_2$** feature just below **X** on the left. In contrast, S_1 slopes upward in all directions from the crossing. The gradient

(18) Rentzepis, P. M. *Chem. Phys. Lett.* **1969**, *3*, 717−720.
(19) By varying the hypersphere radius[13] (Supporting Information, Table S1).

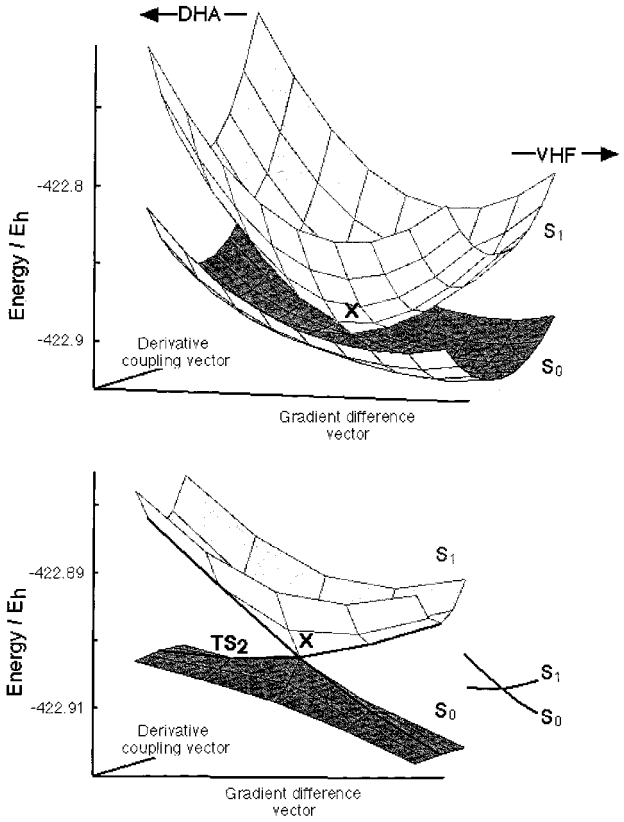

Figure 8. The shape of the ground-state (S_0) and excited-state (S_1) potential energy surfaces in the region of the lowest-energy point on the conical intersection **X** (Figure 5). Both views show that the S_0 surface slopes toward the VHF minimum on S_0. Grid obtained by linear interpolations along the gradient difference and derivative coupling coordinates. Note that, because these coordinates do not involve twisting about the central σ bond, the directions indicated toward DHA and VHF on S_0 (top of figure) are approximate.

difference vector (Figure 5) is the lowest-energy pathway from $\mathbf{M_{VHF}} \rightarrow \mathbf{X}$ on S_1, at the bottom of a deep channel generated by the derivative coupling. We therefore expect the initial motion on S_1 from the $\mathbf{M_{VHF}}$ geometry to be strongly directed toward the crossing **X**. Here, there are three possibilities, all leading back to VHF: (i) Cross to S_0, but be reflected (Scheme 5) and end up as VHF. (ii) There is a small probability that crossing will not take place on the first pass through the crossing region. In this case, the molecule encounters the barrier on S_1, turns, and crosses onto S_0 headed directly for VHF. (iii) There is also the possibility of recrossing to S_1 after (i), which would lead to oscillations in population transfer from $S_1 \rightarrow S_0$.[20] Figure 8 shows that the slope in the derivative coupling coordinate is shallower on S_0 as compared with that of S_1, and the crossing will therefore be easier to "miss" on the return (at least as compared with the same motion on S_1). This is discussed more fully in subsection VI, which describes our dynamics calculations.

IV. Origin of the S_1/S_0 Crossing. The crossing **X** (Figure 5) closely resembles a point located on the S_1/S_0 crossing seam of fulvene;[7b] the rings have the same geometry, but for **2a** the weakly coupled exocyclic group is now a three-electron allyl, instead of the single-electron methylene in fulvene. To understand the origin of the crossing **X**, we can view both **2a** and fulvene as cyclopentadienyl[7c] (**3**, Scheme 6) radicals perturbed by a weakly-coupled exocyclic group. It turns out that the topological features near the S_1/S_0 crossing are analogous.

Scheme 6

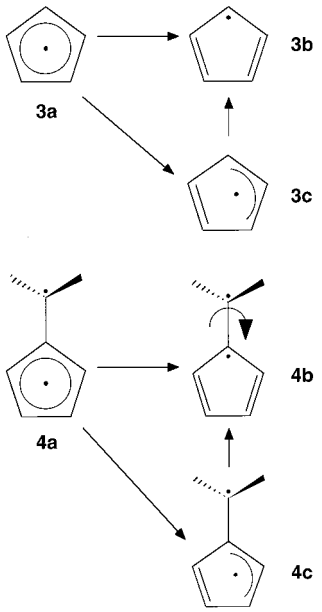

The cyclopentadienyl[7c,21,22] radical is a Jahn−Teller system: a conical intersection enforced by symmetry. Here, the D_0 and D_1 states are degenerate (intersect) at D_{5h} geometries, and the lowest energy point on this intersection (**3a**, Scheme 6) has five equal C−C bond lengths of 1.42 Å.[7c,21] Two types of critical points can be found on the ground state by following the coordinates that lift the degeneracy at this crossing. One is a dienylic minimum (**3b**) having two localized double bonds and an unpaired electron. The other is an allylic transition structure (**3c**) a few cm^{-1} higher in energy, with an allyl group and one localized double bond. The transition structure is for in-plane rearrangement of two equivalent dienylic minima.

In fulvene,[7b] the lowest-energy point on the S_1/S_0 intersection is found when the π-systems of the methylene group and cyclopentadienyl ring are perpendicular to each other (**4a**, Scheme 6). Because the two groups are then perfectly decoupled, this perpendicular point on the S_1/S_0 crossing of fulvene correlates directly with the Jahn−Teller intersection of the cyclopentadienyl radical. Two types of critical points were again found on the ground state near the crossing, with ring geometries the same as in cyclopentadienyl. As expected, there is an allylic transition structure (**4c**) for interconverting dienylic structures (**4b**). However, these dienylic structures are *not* minima in fulvene; they are transition structures for rotation of the exocyclic group. The directions that lift the degeneracy at the S_1/S_0 intersection in fulvene do not involve this rotation, which means that the crossing is found for all rotation angles including planar (0°), when the two groups are weakly coupled.

In the case of VHF (**2a**), because the allyl group and the ring π-systems are twisted but not perpendicular at **X** (Figure 5),

(20) (a) Rose, T. S.; Rosker, M. J.; Zewail, A. H. *J. Chem. Phys.* **1988**, *88*, 6672. (b) Rose, T. S.; Rosker, M. J.; Zewail, A. H. *J. Chem. Phys.* **1989**, *91*, 7415. (c) Zewail, A. H. *J. Phys. Chem. A* **2000**, *104*, 5660−5694.

(21) Borden, W. T.; Davidson, E. R. *J. Am. Chem. Soc.* **1979**, *101*, 3771−3775.

(22) (a) Yu, L.; Foster, S. C.; Williamson, J. M.; Heaven, M. C.; Miller, T. A. *J. Phys. Chem.* **1988**, *92*, 4263−4266. (b) Yu, L. A.; Cullin, D. W.; Williamson, J. M.; Miller, T. A. *J. Chem. Phys.* **1993**, *98*, 2682−2698. (c) Applegate, B. E.; Miller, T. A.; Barckholtz, T. A. *J. Chem. Phys.* **2001**, *114*, 4855−4868. (d) Applegate, B. E.; Bezant, A. J.; Miller, T. A. *J. Chem. Phys.* **2001**, *114*, 4869−4882.

Table 4. CASSCF(8,8)/4-31G Energies of the 5-Carbon Ring System Including Cyano Groups **2b** (Scheme 2) at 4-31G Optimized Geometries (Supporting Figure S8)[a]

geometry	figure	S_0/E_h	S_1/E_h	$\Delta E(S_1-S_0)$ /kcal mol^{-1}	$\Delta E(S_0)$ /kcal mol^{-1}	$\Delta E(S_1)$ /kcal mol^{-1}
$\mathbf{M_{DHA}}$ $\mathbf{S_0}$	S8	−606.12877	−605.91911	131.6	0.0	34.9
		−606.12420	*−605.91693*	*130.1*	*0.0*	*29.6*
$\mathbf{M_{VHF}}$ $\mathbf{S_0}$	S8	−606.14564	−606.00962	85.4	−10.6	−21.9
		−606.00962	*−606.00635*	*84.4*	*−10.5*	*−26.5*
M* $\mathbf{S_1}$	S8	−606.07798	−605.97471	64.8	31.9	0.0
		−606.07562	*−605.96408*	*70.0*	*30.5*	*0.0*
TS* $\mathbf{S_1}$	S8	−606.06395	−605.96312	63.3	40.7	7.3
		−606.06056	*−605.96059*	*62.7*	*39.9*	*2.2*
X $\mathbf{S_1/S_0}$	S8	*−606.06181*	*−606.06159*	*0.1*	*39.1*	*−61.2*

[a] **M** = minimum; **TS** = transition structure; **X** = conical intersection. State-averaged energies in italics. $\Delta E(S_0)$ and $\Delta E(S_1)$ are calculated with the $\mathbf{M_{DHA}}$ $\mathbf{S_0}$ and **M*** $\mathbf{S_1}$ energies, respectively, as references.

Table 5. CASSCF(10,10)/4-31G Energies of the 7-Carbon Ring System **2c** (Scheme 2) at 4-31G Optimized Geometries (Supporting Figures S9−S12)[a]

geometry	figure	S_0/E_h	S_1/E_h	$\Delta E(S_1-S_0)$ /kcal mol^{-1}	$\Delta E(S_0)$ /kcal mol^{-1}	$\Delta E(S_1)$ /kcal mol^{-1}
$\mathbf{M_{DHA}}$ $\mathbf{S_0}$	S9	−499.79146	−499.59470	123.5	0.0	35.0
		−499.78732	*−499.59280*	*122.1*	*0.0*	*35.5*
$\mathbf{TS_1}$ $\mathbf{S_0}$	S9	−499.71285	−499.67346	24.7	49.3	−14.4
		−499.71031	*−499.67141*	*24.4*	*48.3*	*−13.9*
$\mathbf{M_{VHF}}$ $\mathbf{S_0}$	S9	−499.78444	−499.61814	104.4	4.4	20.3
		−499.77915	*−499.61461*	*103.2*	*5.1*	*21.8*
M* $\mathbf{S_1}$	S10	−499.75507	−499.65047	65.6	22.8	0.0
		−499.75314	*−499.64931*	*65.2*	*21.4*	*0.0*
TS* $\mathbf{S_1}$	S10	−499.71248	−499.63770	46.9	49.6	8.0
		−499.71024	*−499.63607*	*46.5*	*48.4*	*8.3*
$\mathbf{XS_1/S_0}$	S11	*−499.72404*	*−499.72398*	*<0.1*	*39.7*	*−46.1*
$\mathbf{TS_2}$ $\mathbf{S_0}$	S12	−499.73089	−499.70348	17.2	38.0	−33.3
		−499.72881	*−499.70189*	*16.9*	*36.7*	*−33.0*
$\mathbf{TS_3}$ $\mathbf{S_0}$	S12	−499.73179	−499.70258	18.3	37.4	−32.7
		−499.72968	*−499.70097*	*18.0*	*36.2*	*−32.4*

[a] **M** = minimum; **TS** = transition structure; **X** = conical intersection. State-averaged energies in italics. $\Delta E(S_0)$ and $\Delta E(S_1)$ are calculated with the $\mathbf{M_{DHA}}$ $\mathbf{S_0}$ and **M*** $\mathbf{S_1}$ energies, respectively, as references.

the two π-systems are weakly coupled. This explains why the π electrons are not uniformly delocalized in the fulvene ring at **X**, as they are at the D_{5h} cyclopentadienyl crossing.[7c,21,22c] Figure 7 shows the two critical points found on S_0 near **X** for **2a**. These are both transition structures, just as in fulvene.[7b] $\mathbf{TS_2}$ correlates with the allylic transition structure for in-plane rearrangement of cyclopentadienyl **3c**; $\mathbf{TS_3}$ correlates with the dienylic cyclopentadienyl minimum **3b**, which is a transition structure for rotation of the exocyclic group as in fulvene **4b**.

V. Justifying the Model System 2a. The 4-31G basis set was used for CASSCF calculations on model systems **2b** and **2c**, as there was little change in relative energies or geometries on going to the cc-pVDZ basis for **2a**.

Energies for ground- and excited-state structures of **2b** and **2c** are given in Tables 4 and 5. The structures themselves are illustrated in the Supporting Information (Figures S8−S12), as there are no significant differences from the corresponding structures for **2a** discussed above. This in itself gives us confidence that the potential energy surface of the title compound **1** will also have the same topology as **2a**.

The effect of including the cyano groups in the CASSCF active space was tested for **2b**. Single point energy calculations were carried out for the S_1 state at the **M*** geometry and the S_0 state at the $\mathbf{M_{DHA}}$ geometry, with 12 electrons in 12 orbitals including the cyano groups, using the 4-31G basis set. In both cases, the occupations of the four cyano group orbitals were around 1.93 and 0.07. These occupations are a little different from 2.0 (occupied) and 0.0 (unoccupied), suggesting initially that these orbitals belong in the active space. However, in this work we are only concerned with the *changes* in the electron distribution on going from S_0 to S_1. Since the occupations of the cyano group orbitals do not change then, we can safely leave them out of the active space. This was further tested by reoptimizing the **M*** $\mathbf{S_1}$ geometry with the cyano groups in the active space and finding that the only change was that the CN bond lengths increased by 0.01 Å. However, since all orbitals are fully optimized in the calculation, the cyano groups can indirectly affect the smaller active space for **2b** and, hence, the relative energies of the ground[23b] and excited states (inductive effect).

For **2b**, the conical intersection **X** was found to be the lowest-energy point on S_1 by ∼60 kcal mol^{-1} (Table 4), and $\mathbf{M_{VHF}}$ was found to be ∼10 kcal mol^{-1} lower in energy than $\mathbf{M_{DHA}}$ with CASSCF/4-31G. $\mathbf{M_{VHF}}$ for **2b** is still lower in energy than $\mathbf{M_{DHA}}$ with B3LYP/cc-pVDZ, although the difference is now reduced to ∼5 kcal mol^{-1} (Table 3). Otherwise, the calculated relative energetics of **2a** (Table 1) and **2b** are very much the same. In particular, the vertical excitation energies at $\mathbf{M_{DHA}}$ and $\mathbf{M_{VHF}}$ agree to within ±2 kcal mol^{-1}; the same red shift in the absorption spectra is predicted in both cases.

For **2c** (seven-membered heptafulvene ring), $\mathbf{M_{DHA}}$ is the lowest-energy S_0 isomer by ∼4 kcal mol^{-1} with CASSCF/4-

(23) (a) Daub, J.; Gierisch, S.; Klement, U.; Knöchel, T.; Maas, G.; Seitz, U. *Chem. Ber.* **1986**, *119*, 2631−2646. (b) Experimentally, if one cyano group is replaced by an ester group, the thermal back reaction is much faster: Bross, P. A. Thesis, Regensburg University, 1992.

Table 6. Transition Energies and Oscillator Strengths for DHA and VHF, Calculated Using TDDFT (B3LYP/cc-pVDZ) at B3LYP/cc-pVDZ Optimized S_0 Geometries (Supporting Figure S13; S_0 Energies in Table 3)[a]

system	structure	ΔE_{CASSCF} $S_0 \rightarrow S_1$	ΔE_{TDDFT} $S_0 \rightarrow S_1$	f_{TDDFT} $S_0 \rightarrow S_1$	ΔE_{TDDFT} $S_0 \rightarrow S_2$	f_{TDDFT} $S_0 \rightarrow S_2$
1	$\mathbf{M_{DHA}}$		3.51	0.159	4.34	0.011
	$\mathbf{M_{VHF}}$		2.23	0.003	2.88	0.487
2a	$\mathbf{M_{DHA}}$	5.76	3.84	0.172	5.12	0.003
	$\mathbf{M_{VHF}}$	3.73	2.71	0.002	3.94	0.408
2b	$\mathbf{M_{DHA}}$	5.70	3.78	0.151	4.83	0.005
	$\mathbf{M_{VHF}}$	3.70	2.11	0.000	3.48	0.429
2c	$\mathbf{M_{DHA}}$	5.35	3.49	0.181	4.38	0.003
	$\mathbf{M_{VHF}}$	4.53	2.43	0.004	3.56	0.434

[a] Energy differences are in eV.

31G (Table 5), becoming 14 kcal mol^{-1} lower with B3LYP/cc-pVDZ (Table 3). This ordering agrees with the experiment.[23] All of the critical points located for **2a** were found for **2c**; the potential energy surfaces have the same topology. However, the effects on the energetics are not exactly additive; $\mathbf{M_{VHF}}$ for **1** (seven-membered ring and cyano groups) is calculated to be ~3 kcal mol^{-1} more stable than $\mathbf{M_{DHA}}$ (Table 3).

Finally, TDDFT[12b,c] calculations have been performed on the three model systems **2a**−**c** (Scheme 2) and the real system **1** (Scheme 1) at optimized B3LYP/cc-pVDZ geometries, to characterize the first excited state of DHA and VHF (Table 6). The $S_0 \rightarrow S_1$ transition is dominated by the HOMO → LUMO excitation in each case. S_1 is therefore calculated to be the same for model (**2a**−**c**) and real (**1**) systems, confirming that the model studies are valid. For CASSCF, the $S_0 \rightarrow S_1$ transition involves a mixture of a single and a double excitation in DHA and a single excitation in VHF. The single excitations are the same as those found with TDDFT, showing that we are calculating S_1 to be the same state with CASSCF and TDDFT.

For VHF, the experimental $S_0 \rightarrow S_1$ absorption is in the visible region (~480 nm, 2.6 eV).[5] This is mid-way between the calculated $S_0 \rightarrow S_1$ (2.23 eV) and $S_0 \rightarrow S_2$ (2.88 eV) transitions for system **1** (Table 6). However, the $S_0 \rightarrow S_1$ transition is calculated to be much weaker ($f = 0.003$) than that of $S_0 \rightarrow S_2$ ($f = 0.487$), which suggests that S_2 may also be pumped experimentally.

VI. Model Trajectory Calculations. In subsections I−III, we argued that the shape of the S_1 and S_0 potential energy surfaces around the conical intersection explains the irreversibility of the photochemical ring-opening reaction from DHA to VHF. The effects of nuclear kinetic energy were suggested, and the purpose of the dynamics calculations described here was to test these suggestions and not to carry out a full dynamics study.

Because ab initio dynamics calculations for molecules as large as **2a** are so time-consuming at present, only two representative model trajectories were run: one for DHA, and one for VHF. The DHA trajectory (Figure 9) was started from the transition structure **TS***, which separates the DHA-like minimum **M*** from the VHF-like conical intersection on S_1. Initial conditions were defined as follows: an energy of 3 kcal mol^{-1} was given to the vibrational coordinate corresponding to the transition vector, in the direction of the conical intersection. (This corresponds to selecting a trajectory which has passed through the reaction bottleneck formed by the transition structure, a procedure we[24] and others[25] have used previously.) The vibrational energies along the other modes were fixed to zero initially. For this trajectory, the energy (−422.828 E_h) and geometry (Figure 9, top) of the point at which decay to S_0 occurred confirm that DHA excitation leads to decay at a higher-energy region of the crossing similar to that of $\mathbf{X}_{early}$ (Figure 6, Table 1). The probabilities[14e] plotted at the bottom of Figure 9 show that decay took place essentially diabatically, 16 fs after leaving **TS***, at a point where the gap between S_1 and S_0 was 5.6 kcal mol^{-1}. The 16 fs time to decay cannot be compared with the experimental lifetime directly, as we have selected one trajectory that has gone through the transition structure with momentum in the right direction. Because this is not the same direction as initial relaxation from the Franck−Condon geometry, we cannot say how long it would take for this trajectory to have reached **TS*** after excitation to S_1. The final photoproduct obtained was a distorted version of $\mathbf{M_{VHF}}$, which supports the assumption that this isomer is favored for inertial reasons and that, after excitation of DHA, decay is unlikely to lead back to DHA on S_0.[26]

The VHF trajectory (Figure 10) was started from the $\mathbf{M_{VHF}}$ geometry on S_1, the Franck−Condon geometry. The kinetic energy in all of the vibrational modes was set to zero initially, but it increased rapidly along the reaction coordinate because the S_1 surface is so steeply sloped. Figure 10 shows that decay to S_0 takes place within 8 fs. The S_1 and S_0 states cross at an energy of −422.876 E_h, but decay does not occur until the next step, at which the S_1-S_0 gap has increased to ~6 kcal mol^{-1}.[27] The geometry of the decay point is shown top left in Figure 10. It has an S_1 energy of −422.860 E_h, ~27 kcal mol^{-1} above the lowest-energy point on the crossing (Table 1). Moreover, the gradients on S_1 and S_0 appear to be nearly parallel at this point (Figure 10), whereas the lowest-energy point on the crossing **X** has the shape of an inverted peak on S_1 as shown in Figure 8. Contrasting the hop geometry (Figure 10) with **X** (Figure 5) and the initial geometry $\mathbf{M_{VHF}}$ (Figure 3) suggests an explanation. At **X**, the two rings are almost perpendicular; at $\mathbf{M_{VHF}}$, they are much closer to planar. Because the trajectory reaches the crossing so rapidly, there is no time for torsional relaxation to take place. Instead, relaxation is dominated by in-plane bonding changes within the π-system. Figures 3, 8, and 10 show that these changes on going from $\mathbf{M_{VHF}}$ to the hop geometry are an exaggerated version of the same changes from $\mathbf{M_{VHF}}$ to **X**. As discussed above (subsection II), the crossing does not depend on the torsional angle between the two rings, and higher-energy points on the crossing can therefore be reached at near-planar geometries such as the one at which the hop took place in Figure 10.

(24) Deumal, M.; Bearpark, M. J.; Smith, B. R.; Olivucci, M.; Bernardi, F.; Robb, M. A. *J. Org. Chem.* **1998**, *63*, 4594−4600.
(25) Carpenter, B. K. *Angew. Chem., Int. Ed.* **1998**, *37*, 3341−3350.
(26) In these model trajectory calculations, both DHA and VHF decay at crossing points above the minimum, but for very different reasons. Decay from the DHA side will always take place in a higher energy region of the crossing, regardless of the kinetic energy available, because the S_1 reaction path is not in the branching space which lifts the degeneracy (Results and Discussion, subsection II). In contrast, the S_1 reaction path from VHF is in the branching space and does lead to the crossing minimum **X** (Results and Discussion, subsection III). However, the kinetic energy derived from in-plane bond relaxation means that the hop takes place before torsional relaxation is complete, in a higher energy region of the crossing.
(27) The energy gaps at the hop geometry are approximately the same for both model trajectories, but appear different in Figures 9 and 10 because the vertical scales differ.

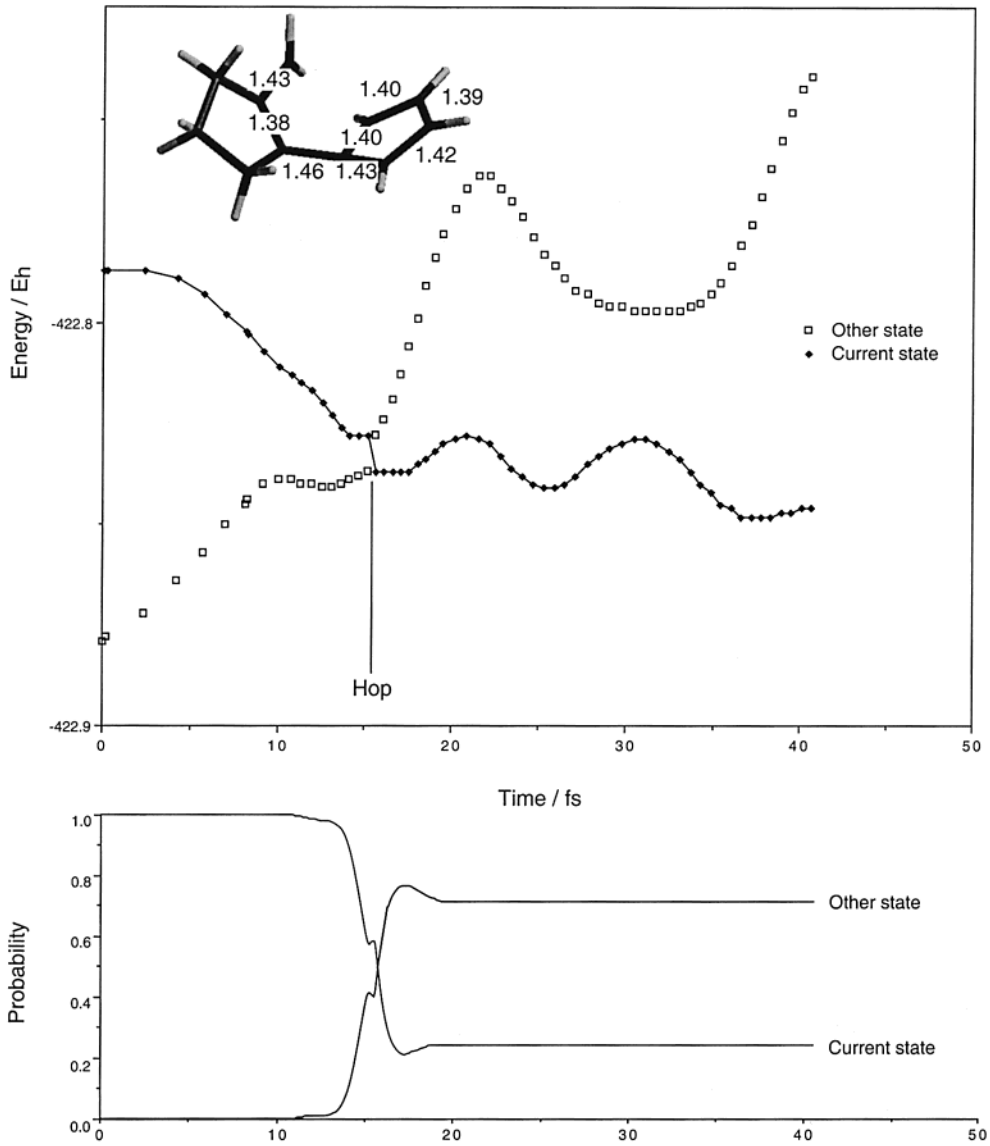

Figure 9. Trajectory started at the **TS*** geometry on S_1 for **2a** (4-31G basis): electronic energy of the S_0 and S_1 states plotted against time (top) and probability that a particular state is occupied (bottom). Initial momentum was directed along the **TS*** transition vector toward the S_1/S_0 crossing as discussed in the text. "Current state" is initially S_1, but becomes S_0 after the hop that occurs at the geometry indicated at the top of the figure (all bond lengths are in Å).

The path followed by the VHF trajectory is different from the path suggested by Figure 8, which shows the changes in energy along the gradient difference and derivative coupling vectors starting at **X**, where the rings are near-perpendicular. Figure 10 is a trajectory for an isolated molecule. In a solvent, some kinetic energy will be lost as heat to the surroundings, and therefore the "real" reaction path to the crossing will be somewhere between those suggested by Figures 8 and 10.

After the hop has taken place, Figure 10 shows that the energy of the two states rises, mirroring Scheme 5/Figure 2. There is insufficient energy to overcome the steep barrier on S_0, and the molecule is directed back toward the S_0/S_1 crossing, which it reaches after 15 fs. Recrossing to S_1 could therefore take place, suggesting that coherent oscillations in population transfer to the ground state (such as those observed in, e.g., NaI,[20] azulene,[7a,28] and bacteriorhodopsin[29]) might be observed experimentally. For the VHF trajectory calculation, recrossing was disabled, partly because it was unexpected, but mostly because we were trying to determine the product on S_0 (the distorted VHF shown top right of Figure 10; cf. Figure 3). In this calculation, all of the momentum developed along a coordinate leading directly to the crossing, and there was insufficient time for redistribution into other vibrational modes to take place to avoid a direct re-encounter with the crossing after turning on S_0. In a realistic simulation, vibrations orthogonal to the reaction coordinate would cause some of the population to avoid the crossing and remain on S_0.

The ultrafast decay from VHF has not been studied explicitly to date. Decay from DHA, which was observed on the picosecond time scale,[5] would not be expected to give oscillations in population transfer as there is no restoring force on S_0

(28) (a) Wurzer, A. J.; Wilhelm, T.; Piel, J.; Riedle, E. *Chem. Phys. Lett.* **1999**, *299*, 296−302. (b) Diau, E. W.-G.; De Feyter, S.; Zewail, A. H. *J. Chem. Phys.* **1999**, *110*, 9785−9788.

(29) (a) Schoenlein, R. W.; Peteanu, L. A.; Mathies, R. A.; Shank, C. V. *Science* **1991**, *254*, 412. (b) Kochendoerfer, G. G.; Mathies, R. A. *J. Phys. Chem.* **1996**, *100*, 14526. (c) Wang, Q.; Schoenlein, R. W.; Peteannu, L. A.; Mathies, R. A.; Shank, C. V. *Science* **1994**, *266*, 422.

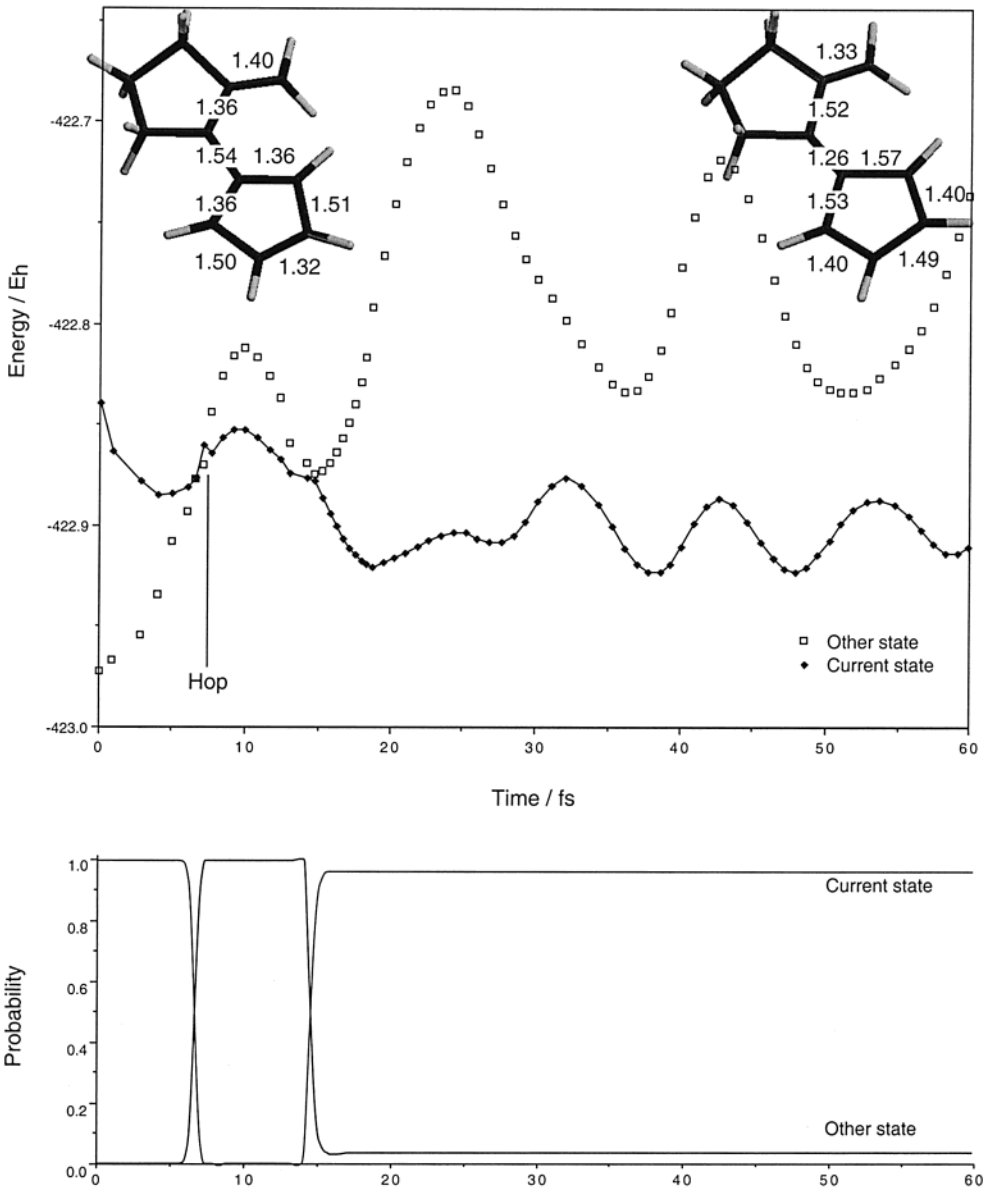

Figure 10. Trajectory started at the $\mathbf{M_{VHF}}$ geometry on S_1 for **2a** (4-31G basis): electronic energy of the S_0 and S_1 states plotted against time (top) and probability that a particular state is occupied (bottom). There was no initial momentum. "Current state" is initially S_1, but becomes S_0 after the hop at the geometry indicated at the top left of the figure. The geometry at the top right is the distorted VHF structure on S_0 obtained when the trajectory calculation was terminated (all bond lengths are in Å).

directing molecules back toward the crossing. The fundamental asymmetry of the DHA/VHF system could therefore be confirmed experimentally.

Conclusions

Dihydroazulene (DHA)/vinylheptafulvene (VHF) photochromism was investigated by studying the isomerization of 1,2,3,8a,9-pentahydrocyclopent[a]azulene-9,9-dicarbonitrile **1** through CASSCF calculations on the ground (S_0) and first excited (S_1) states of the smaller model compounds **2a**−**2c**. The fact that the topology of the ground- and excited-state potential energy surfaces is the same for all three model systems gives us confidence that we have a good description of the behavior of **1** itself.

The S_1 reaction coordinate is characterized by a transition structure for adiabatic ring opening, connecting a DHA-like intermediate to a much more stable VHF-like conical intersection between S_1 and S_0. This crossing is responsible for the rapid, barrier-activated decay of DHA (as suggested in ref 5) and also the lack of fluorescence at any temperature from the resulting VHF. Because the S_0 potential energy surface slopes steeply toward VHF at the crossing (Figures 2 and 8), excitation of both DHA and VHF produces only VHF; that is, the isomerization is photochemically "one-way". The shape of the crossing therefore explains the quantum yield approaching 1.0 for DHA → VHF conversion measured in ref 5. Any molecule with the same potential energy surface topology will give similar irreversible photochromism, and we expect that other examples will be found or eventually designed.

The product may be the same, but after excitation of DHA and VHF, decay takes place in different regions of the S_1/S_0 crossing. This was explained by the fact that the minimum energy path from VHF on S_1 lies in the branching space of the intersection and therefore can lead to the lowest-energy point

on the crossing. For DHA, the reaction coordinate is independent of the branching space and hence reaches the crossing at a much higher energy. We therefore need at least three coordinates to properly describe reaction pathways on S_1 and S_0; a single plot of energy against "reaction coordinate" is misleading.

Different routes to the crossing lead to clear differences in the probability of recrossing back onto S_1 that should be testable experimentally. From DHA, the crossing is reached along a reaction path that leads directly to VHF on S_0, and hence there will be no recrossing to S_1 after decay. The rate-determining step here is overcoming the barrier on S_1. For VHF, however, a steep barrier on both S_0 and S_1 blocks the path to DHA. From VHF, the crossing is effectively "sloped",[10] and recrossing to S_1 is possible before eventually returning to VHF on S_0. This may be observable as oscillations in population transfer with coherent femtosecond spectroscopy,[20,28,29] in contrast to decay from DHA.

Acknowledgment. This research was supported by the European Union. Many thanks to Marc Zeedar for Z-Write, Michael Klene for assistance with Gnuplot and Figure 8, and Dr. Jörg Daub for suggesting the problem. All calculations were run on an IBM SP2 using development versions of the Gaussian 99 program.

Supporting Information Available: Figures S1−S13 and Scheme S1 showing the geometries of critical points located for model systems **2b** and **2c**, and additional illustrations of reaction paths for **2a** (PDF). This material is available free of charge via the Internet at http://pubs.acs.org.

JA0161655